Astron. Astrophys. 288, 883–896 (1994)

ASTRONOMY AND ASTROPHYSICS

Multiple scattering of polarized radiation in circumstellar dust shells

N.V. Voshchinnikov[1]* **and V.V. Karjukin**[2]

[1] Max-Planck-Gesellschaft, AG "Staub in Sternentstehungsgebieten", Schillergäßchen 3, D-07745 Jena, Germany
[2] Laboratory of Statistical Modelling, Institute of Mathematics and Mechanics, St. Petersburg University, St. Petersburg-Petrodvoretz, 198904 Russia

Received 24 September 1993 / Accepted 14 February 1994

Abstract. On the basis of recently developed modification of the Monte Carlo approach (the method of symmetrized trajectories), a numerical code for the transfer of the polarized radiation in circumstellar shells has been created. This code allows to study light scattering by dust grains in prolate or oblate spheroidal shells of a moderate optical thickness ($\tau \lesssim 5 - 8$) seen at various angles. The description of the Monte Carlo approach and various tests are presented. The extensive calculations were performed for the cases of Rayleigh scattering (grain albedo $\Lambda = 0.1, 0.5$, and 1.0) and Mie scattering (silicate-graphite mixtures, wavelength range 1000 Å - 1 μm). The dependencies of the intensity and polarization on the parameters of dust grains and homogeneous circumstellar shells are examined.

It was found that the light scattered by circumstellar dust is a noticeable fraction of the observed stellar radiation in the visual and ultraviolet spectral regions. The fraction of scattered radiation grows with increasing Λ and decreasing the shell semiaxis ratio. The ratio of the scattered radiation intensity to the direct stellar one has a maximum at about 2000 - 3000 Å and can reach $I_{\rm sca}/I_* \approx 0.3$ - 0.4 for the uniform oblate spheroidal shell. In some cases, the summary influence of the scattered radiation and the circumstellar (and interstellar) extinction can produce the wavelength independent extinction curves. Such curves cannot be analyzed by the colour-excess method.

The degree of linear polarization usually does not exceed 1 - 2 % and has a weak wavelength dependence in the visual and red regions of the spectrum. At the ultraviolet wavelengths, the polarization has a maximum in the region of the bump ($\lambda \approx$ 2200 Å) and a minimum at $\lambda \approx$ 1800 - 2000 Å.

We have also considered the case of the screening of stellar radiation by dense circumstellar clouds which occurs for some young stars (e.g., Herbig Ae/Be stars). If only the scattered radiation is observed, the upper limit on the stellar brightness variations is of $1^{\rm m}$ - $2^{\rm m}$ in the ultraviolet and $3^{\rm m}$ - $4^{\rm m}$ in the red wavelength region. The maximum degree of linear polarization grows with increasing wavelength and can reach 8 - 10 %.

Key words: circumstellar matter – radiative transfer – polarization – stars: late-type – stars: pre-main-sequence

1. Introduction

Dust shells surround many stars both young and old. The observed intrinsic polarization indicates an asymmetric distribution of dust grains around those stars. The optical thickness of the circumstellar (CS) shells may be large, especially in the far-ultraviolet region. Thus, the theoretical study of the light scattering by CS dust has to include the modelling of the polarized radiation transfer in the non-spherical shells.

The previous models of shells around stars and protostellar objects were mainly focused on the infrared radiation (e.g., Jones & Merrill 1976; Rowan-Robinson & Harris 1982; Gürtler et al. 1991; Berrilli et al. 1992; Natta et al. 1993; Hartmann et al. 1993). The shell shape was approximated by sphere because the infrared radiation arises inside a large volume surrounding a central object. The observed infrared polarization of deep-embedded sources may be attributed to the dichroic extinction by non-spherical aligned grains presenting on the line of sight.

With the decrease of the radiation wavelength, the thermal dust emission drops off while the radiation scattered by dust grains begins to play a more important role. The largest fraction of the scattered radiation is produced within the inner layers of the CS shells. The polarization of star light due to dust scattering has been studied on the base of single scattering models (Zellner 1971; Greenberg & Wang 1972; Shawl 1974; Voshchinnikov 1989). The results have been used to account for the observations of late-type and young stars. The models with multiple scattering of polarized radiation have been developed by Angel (1969) for X-ray sources, Daniel (1978, 1980b, 1982) for

Send offprint requests to: N.V. Voshchinnikov (St. Petersburg)
* On leave from Astronomical Institute, St. Petersburg University, St. Petersburg-Petrodvoretz, 198904 Russia,
E-mail: vayak@astro.lgu.spb.su

cool stars, Daniel (1980a) for eclipsing binaries, Höflich (1991) for SN 1987A. These authors used the Monte Carlo simulation and considered electron (Thomson) scattering or Mie scattering by single size grains. Other approaches to the solution of the problem of polarized radiation transfer have been created for plane layer only (see e.g., Hovenier 1971; Hansen & Travies 1974; Sobolev 1975; Loskutov 1990). Such scattering geometry is quite suitable for planetary atmospheres but not for CS shells.

In the recent years, the images and polarization maps of some young (protostellar) objects have been obtained. The observations were made in several spectral bands mainly at visual and near infrared wavelengths. The models developed by Bastien (1988), Bastien & Ménard (1988), Ménard (1989), Whitney & Hartmann (1992), Fischer (1993), Fischer et al. (1993) allow to compare the calculated maps with the observations. However, many of the objects cannot be spatially resolved and we observe the total radiation of the star and CS shell.

In the present paper, we consider the multiple scattering of polarized radiation in CS shells. In order to solve the problem, we use the Monte Carlo approach and present the results for the wide spectral region from near infrared to far ultraviolet. It should also be noted that previous modelling, except for the pioneering work of Greenberg & Wang (1972), dealt with the visual and infrared polarization only. But now the ultraviolet polarization for stars with dust shells have been observed (e.g., Schulte-Ladbeck et al. 1992). The model of the shell and the Monte Carlo scheme used are described in Sect. 2 and Sect. 3, respectively. Section 4 contains the various numerical tests which were made. The results of the calculations for Rayleigh and Mie scattering and their discussion are presented in Sect. 5. In Sect. 6, we summarize our results.

The first numerical results obtained on the basis of the described Monte Carlo code were applied to the consideration of the light scattering in protoplanetary disks around the Herbig Ae/Be stars UX Ori and WW Vul (Voshchinnikov et al. 1993).

2. Model description

In many cases, we see that CS shells are axially symmetric. There are observational evidences for quasi-spherical (from far infrared observations) or disk-like (from near infrared and visual observations) shells around T Tau and Herbig Ae/Be stars (Rydgren & Cohen 1985; Weintraub et al. 1992; Rodriguez et al. 1992). The images of the shells around some late-type stars usually have non-spherical (possibly, elliptical) shape (see e.g., Tamura et al. 1988; Sloan et al. 1993).

We assume that the shape of the CS shell is a prolate or an oblate spheroid (ellipsoid of revolution) with a semiaxis ratio A/B. One source of the non-polarized radiation (star) lies in the center of the shell. We define as i the angle between the rotation axis and the line of sight ($0° \leq i \leq 90°$). The envelope is seen as a circle (pole-on) for $i = 0°$, and as an ellipse (edge-on) for $i = 90°$. Our model can simulate disk-like structures for oblate shells when the ratio A/B is large. The optical thickness of the shell $\tau^{\rm ext}(\lambda)$ is maximal along the main semiaxis (A). Let us define the optical path of the stellar radiation inside the shell in the direction of an observer as $\tau_i^{\rm ext}(\lambda)$. It varies from $\tau_0^{\rm ext}(\lambda) = \tau_{90}^{\rm ext}(\lambda)/(A/B)$ to $\tau_{90}^{\rm ext}(\lambda)$ when i increases from 0° to 90°. We consider the homogeneous CS shells, but a new code is being developed for inhomogeneous shells with a central cavity free of dust.

The optical properties of dust grains (extinction cross-section, albedo and scattering matrix) are calculated preliminary for each wavelength. We assume that the grains scatter the radiation azimuth-independently, which is valid for spherical particles or randomly aligned non-spherical particles. Then, the scattering matrix contains four or six different non-zero elements (see Eq. (7)). Below, we present the results obtained for Mie scattering by homogeneous spheres. We consider silicate-graphite mixtures of grains with the power-law size distribution (MRN mixture; Mathis et al. 1977):

$$n_{\rm Si,C} = K_{\rm Si,C} \cdot n_{\rm H} \cdot a^{-q}. \tag{1}$$

Here, $n_{\rm H}$ is the hydrogen number density and the coefficients $K_{\rm Si}$ and $K_{\rm C}$ are determined from the cosmic abundance of silicon and carbon. The parameters of the dust grains mixtures are: the minimum (a_-) and the maximum (a_+) radii of particles, the index q in Eq. (1), and the ratio of number densities of silicate and graphite grains $n_{\rm Si}/n_{\rm C} = K_{\rm Si}/K_{\rm C}$.

In order to test the Monte Carlo code and to clarify the dependence of the observable quantities on the model parameters, we have also performed some calculations for Rayleigh scattering.

3. Monte Carlo approach and its features

The Monte Carlo method is the most suitable approach to solve the problem of multiple scattering of polarized radiation for non-spherical envelope.

The equation for the radiation transport can be written in the standard form (see e.g., Chandrasekhar 1950; Sobolev 1975)

$$\boldsymbol{\omega} \cdot \nabla \boldsymbol{S}(\boldsymbol{r}, \boldsymbol{\omega}) + \boldsymbol{S}(\boldsymbol{r}, \boldsymbol{\omega})$$

$$= \frac{\Lambda}{4\pi} \int \boldsymbol{P}(\boldsymbol{\omega}, \boldsymbol{\omega}') \boldsymbol{S}(\boldsymbol{r}, \boldsymbol{\omega}') d\omega' + \boldsymbol{F}(\boldsymbol{r}, \boldsymbol{\omega}), \tag{2}$$

where $\boldsymbol{S} = (I, Q, U, V)$ is the Stokes vector, $\boldsymbol{r} = (x, y, z)$ is the photon radius-vector (star is at the center of the Cartesian coordinate system x, y, z), the unit vector $\boldsymbol{\omega} = (\omega_{\rm x}, \omega_{\rm y}, \omega_{\rm z})$ defines the direction of the photon walk, Λ is the albedo of dust grains, and $\boldsymbol{F}$ is the source of photons (star). We assume that the radiation does not fall on the shell outside.

For particles considered, the matrix $\boldsymbol{P}(...)$ depends only on the scattering angle Θ ($\mu = \cos\Theta = (\boldsymbol{\omega}, \boldsymbol{\omega}')$) and can be represented as

$$\boldsymbol{P}(\mu) = \boldsymbol{L}(\pi - \nu_2) \boldsymbol{R}(\mu) \boldsymbol{L}(-\nu_1), \tag{3}$$

where $\boldsymbol{L}(\nu)$ is the rotation matrix and $\boldsymbol{R}(\mu)$ is the scattering matrix. The matrix of rotation $\boldsymbol{L}(\nu)$ is

$$\boldsymbol{L}(\nu) = \begin{pmatrix} 1 & 0 & 0 & 0 \\ 0 & \cos 2\nu & \sin 2\nu & 0 \\ 0 & -\sin 2\nu & \cos 2\nu & 0 \\ 0 & 0 & 0 & 1 \end{pmatrix}, \tag{4}$$

where ν_1 and ν_2 are the angles between the scattering plane and the planes containing the z'−axis of the auxiliary Cartesian coordinate system and the vectors $\boldsymbol{\omega}$ or $\boldsymbol{\omega}'$, respectively. The elements of the matrix $\boldsymbol{L}(\nu)$ can be calculated with the use the formulae of the spherical trigonometry. We take into account the changes of the signs for the angles ν_1 and ν_2 due to the change of the rotation direction from the plane $z'O\omega'$ to the plane $z'O\omega$ around the axis Oz' (see Figs. 2 and 3 in the paper of Hovenier & van der Mee 1983 for details). The use of the auxiliary system is connected with the non-invariant of Stokes vector relative to the rotation (see Chandrasekhar 1950 or Marchuk et al. 1980). Since we observe the shell from infinity in the direction $-\boldsymbol{\omega}^\circ$, the auxiliary system has been chosen in such a way that the direction of the z'−axis coincides with the direction $\boldsymbol{\omega}^\circ$ (and the z−axis). Then the symmetrized trajectories can be easily constructed.

The first element of $\boldsymbol{R}(\mu)$ is normalized by the unity

$$\frac{1}{2}\int_{-1}^{1} R_{11}(\mu)d\mu = 1. \tag{5}$$

In the case of Rayleigh scattering, we have

$$\boldsymbol{R}(\mu) = \frac{3}{2}\begin{pmatrix} (1+\mu^2)/2 & -(1-\mu^2)/2 & 0 & 0 \\ -(1-\mu^2)/2 & (1+\mu^2)/2 & 0 & 0 \\ 0 & 0 & \mu & 0 \\ 0 & 0 & 0 & \mu \end{pmatrix}. \tag{6}$$

In the case of Mie scattering, the matrix $\boldsymbol{R}(\mu)$ can be written as follows:

$$\boldsymbol{R}(\mu) = \begin{pmatrix} R_{11} & R_{12} & 0 & 0 \\ R_{12} & R_{11} & 0 & 0 \\ 0 & 0 & R_{33} & R_{34} \\ 0 & 0 & -R_{34} & R_{33} \end{pmatrix}. \tag{7}$$

As a result of the solution of Eq. (2), we derive the Stokes vector for the total radiation from the star and the shell propagating in the direction of the observer $\boldsymbol{\omega}^\circ$. The components of the Stokes vector can be transformed to the degree of linear polarization

$$P = \frac{\sqrt{Q^2+U^2}}{I}, \tag{8}$$

the direction of linear polarization

$$\tan 2\vartheta = \frac{U}{Q} \tag{9}$$

and the degree of circular polarization

$$q_V = \frac{V}{I}. \tag{10}$$

The sign of the angle ϑ is chosen in such a way that $\cos 2\vartheta$ has the same sign as Q.

We define that the polarization is positive if its direction is perpendicular to the major semiaxis of the spheroidal shell A (equatorial polarization), and the polarization is negative if it is parallel to A (polar polarization).

It should be noted that we can distinguish the stellar radiation and the scattered radiation after each scattering which may be useful to test the Monte Carlo code and to clarify the effects of the multiple scattering in CS shells.

In order to solve the radiation transfer problem, we use the following special technique of the Monte Carlo method.

(a). We consider a scalar transport process (without polarization) and use the vector weight coefficients to describe the polarized radiation. Sobol' (1973) has proposed such a vector scheme and Marchuk et al. (1980) have used it to consider the polarized radiation transfer in the terrestrial atmosphere.

(b). The corresponding weight coefficients are also used to take into account the processes of the photon absorption and escaping out of the shell. As a result, the photon trajectories become infinite, and we have to cut them to stop the photon random walk. For this purpose, we set a number of photon scatterings $N_{\rm scat}$. The value of $N_{\rm scat}$ is chosen after probe calculations.

(c). We consider an isotropic flight of photons from the star. After the first scattering, the modified scheme for the simulation of the direction and the free path length is used. Since a selected direction of the radiation propagation (to the observer) exists and the optical thickness of the CS shells is usually rather small ($\tau \lesssim 5$ - 8), we apply the optimization scheme of Karjukin (1984) with some recently made improvements.

It should be noted that all the features of our Monte Carlo approach are directed to the decrease of the variance (the relative statistical error of the calculations).

Unfortunately, the scheme described above does not allow to achieve good accuracy for reasonable computational time in some cases (for instance, a zero polarization for the spherical shell). In order to overcome this obstacle, one of the authors (V.K.) has developed a special method of symmetrized trajectories. It allows to drop sharply the variance (for fixed number of photons) and the computational time. Below, we present the main idea of this method (see Karjukin 1992 for details).

At each step of the calculations, we construct the main (principal) photon trajectory and an additional (symmetrized) one. For the symmetrized trajectory construction, the method of dependent tests (i.e., the same random numbers as for the main trajectory) is used. If the suggestion about the weight coefficients of the photon escaping out the shell is rejected (see approach (b) mentioned above), then the symmetrized trajectory is the main trajectory rotated at the angle $\phi = \frac{\pi}{2}$ around the vector $\boldsymbol{\omega}^\circ$. If we use the weight coefficients, this method of the symmetrized trajectory construction remains in the case only when the vector $\boldsymbol{\omega}^\circ$ coincides with the symmetry axis of the shell. Given approach leads to zero sum of the random quantities derived for the symmetrized and main trajectories (for the second or third components of the Stokes vector) and consequently to zero variance. Of course, the approach suggested gives zero polarization for the spheroidal shell being observed along the rotation axis. In general case, the scattering angles are equal for the main and symmetrized trajectories but the photon paths are not (they are equal for the spherical shell only).

The computational scheme includes the following steps.

1°. The selection of input parameters: the type of scattering (Rayleigh or Mie), the albedo of Rayleigh particles Λ (or the wavelength dependence of albedo, cross-sections and scattering matrices for Mie scattering), the optical thickness of the shell along the main axis $\tau_{90}^{\rm ext}$ (for Mie scattering, we must also include the wavelength to which corresponds this value), the semiaxis ratio A/B, the angle of observations i, the number of scatterings $N_{\rm scat}$ to be considered, a parameter stopping the calculations (the number of photons $N_{\rm stat}$, computational time, the intensity variance $\sigma_{\rm I}$ or the linear polarization variance $\sigma_{\rm P}$). In the case of Mie scattering, we do all the calculations independently for each wavelength.

2°. The start of a photon walk from the center. The initial coordinates of the main and symmetrized trajectories of the photon and the corresponding random quantities for the Stokes vector are set to be zero

$$x = y = z = x_{\rm s} = y_{\rm s} = z_{\rm s} = 0,$$
$$\xi_{\rm I} = \xi_{\rm Q} = \xi_{\rm U} = \xi_{\rm V} = \xi_{\rm I_s} = \xi_{\rm Q_s} = \xi_{\rm U_s} = \xi_{\rm V_s} = 0, \quad (11)$$

where for the symmetrized trajectory the subscript s is stood.

3°. The simulation of the isotropic process of the photon flight from the star

$$\mu = \mu_{\rm s} = 1 - 2\gamma_1, \quad \phi = 2\pi\gamma_2, \quad \phi_{\rm s} = \phi + \frac{\pi}{2}. \quad (12)$$

Here, $0 \leq \gamma_{\rm i} \leq 1$ are the uniformly distributed random numbers.

4°. The calculations of the photon flight direction

$$\omega_{\rm x} = \sqrt{1-\mu^2}\sin\phi, \quad \omega_{\rm xs} = \sqrt{1-\mu_{\rm s}^2}\sin\phi_{\rm s},$$
$$\omega_{\rm y} = \sqrt{1-\mu^2}\cos\phi, \quad \omega_{\rm ys} = \sqrt{1-\mu_{\rm s}^2}\cos\phi_{\rm s},$$
$$\omega_{\rm z} = \mu, \quad \omega_{\rm zs} = \mu_{\rm s}. \quad (13)$$

5°. The simulation of the length of the photon free path using the exponential law e^{-t}, where $0 \leq t \leq T$ and T is the optical distance to the boundary of the shell in given direction $\boldsymbol{\omega}$. The coordinates of the first scattering point are

$$x = x + t\omega_{\rm x}, \quad y = y + t\omega_{\rm y}, \quad z = z + t\omega_{\rm z}. \quad (14)$$

The similar expressions with the parameters $t_{\rm s}$, $T_{\rm s}$ and $\omega_{\rm s}$ give the coordinates for the symmetrized trajectory.

6°. The calculations of the probability of the photon escaping out the shell in the direction $\boldsymbol{\omega}$ or $\boldsymbol{\omega}_{\rm s}$

$$W_{\rm T} = e^{-T}, \quad W_{\rm T_s} = e^{-T_s}. \quad (15)$$

Then we calculate the vector weight coefficients

$$W_1 = 1 - W_{\rm T}, \quad W_{\rm 1s} = 1 - W_{\rm T_s},$$
$$W_2 = W_3 = W_4 = W_{\rm 2s} = W_{\rm 3s} = W_{\rm 4s} = 0, \quad (16)$$

and the corresponding random quantities

$$\xi_{\rm I} = \xi_{\rm I_s} = e^{-\tau_{\rm i}^{\rm ext}(\lambda)}, \quad \xi_{\rm Q} = ... = \xi_{\rm V_s} = 0. \quad (17)$$

7°. The process of photon scattering: we consider the first scattering for $\mu = (\boldsymbol{\omega}, \boldsymbol{\omega}^\circ)$ and calculate the corresponding angular coefficients, the components of matrix $\boldsymbol{R}(\mu)$, and new weight coefficients

$$W_1' = R_{11}(\mu)W_1 + R_{12}(\mu)C,$$
$$W_2' = [R_{21}(\mu)W_1 + CR_{22}(\mu)]\cos 2\nu_2$$
$$-[R_{33}(\mu)D - CR_{22}(\mu)]\sin 2\nu_2,$$
$$W_3' = [R_{21}(\mu)W_1 + R_{34}(\mu)W_4]\sin 2\nu_2$$
$$+[R_{33}(\mu)D - R_{34}(\mu)W_4]\cos 2\nu_2,$$
$$W_4' = R_{34}(\mu)D + R_{44}(\mu)W_4, \quad (18)$$

where

$$C = W_2\cos 2\nu_1 - W_3\sin 2\nu_1, \quad D = W_2\sin 2\nu_1 + W_3\cos 2\nu_1. \quad (19)$$

The sines and cosines are determined using the direction of the photon propagation.

8°. The calculations of the corresponding contribution to the random quantities $\xi_{\rm Is}, \xi_{\rm Q_s}, ...$ and $\xi_{\rm I_s}, \xi_{\rm Q_s}, ...$.

9°. The simulation of new direction of the photon flight: we determine the azimuthal angle $\phi = \phi_{\rm s} = 2\pi\gamma_1$ and the scattering angle μ

$$\mu = \frac{1}{k}\left[1 - (1+k)\left(\frac{1-k}{1+k}\right)^{\gamma_2}\right], \quad (20)$$

where k is the solution of the equation

$$1 = \frac{\Lambda}{2k}\ln\frac{1+k}{1-k}. \quad (21)$$

Then we calculate new vector weight $\boldsymbol{W}_{\rm new}$ (using Eqs. (18)) and derive vector weight after scattering

$$\boldsymbol{W}' = \boldsymbol{W}_{\rm new}\frac{\Lambda}{2k}(1 - k\mu)\ln\frac{1+k}{1-k}. \quad (22)$$

10°. The calculations of the angular quantities for new optical distance to the shell boundary in the direction of observer, the simulation new photon run, etc.

11°. If the number of scatterings is less than $N_{\rm scat}$, we go back to the step 4°.

12°. If the selected condition to stop the calculations is not satisfied, we go to the step 2°.

13°. The calculations of the components of the Stokes vector $I = (\xi_{\rm I} + \xi_{\rm I_s})/2$, $Q = (\xi_{\rm Q} + \xi_{\rm Q_s})/2, ...$, the polarization degree, etc., and the output of the results.

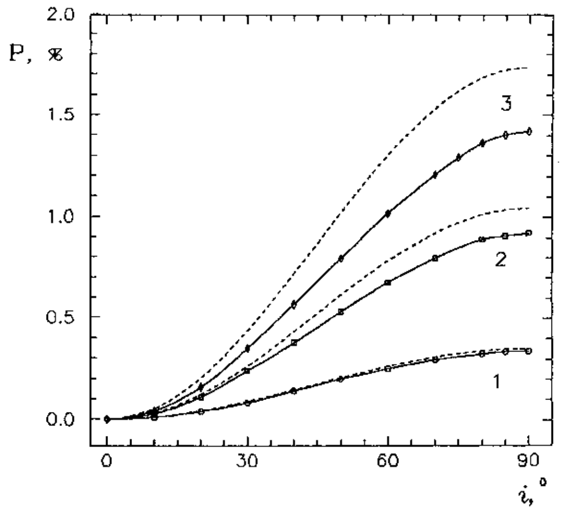

Fig. 1. Polarization degree as a function of the angle of observation (Rayleigh scattering, Λ = 0.5, oblate shell, A/B = 5). Solid lines: Monte Carlo calculations (multiple scattering), dashed lines: analytical approximation for single scattering from Dolginov et al. (1979). 1 — $\tau_{90}^{\rm ext} = 0.1$, 2 — $\tau_{90}^{\rm ext} = 0.3$, 3 — $\tau_{90}^{\rm ext} = 0.5$

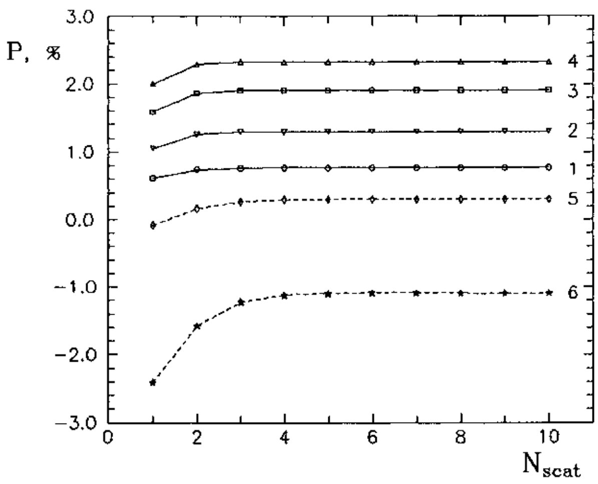

Fig. 2. Polarization degree as a function of the number of scattering (Rayleigh scattering, Λ = 0.5, oblate shell, i = 90°). Solid lines: $\tau_{90}^{\rm ext}$ = 1.0, 1 — A/B = 1.5, 2 — A/B = 2.0, 3 — A/B = 3.0, 4 — A/B = 5.0; dashed lines: 5 — $\tau_{90}^{\rm ext}$ = 3.0, A/B = 2.0, 6 — $\tau_{90}^{\rm ext}$ = 5.0, A/B = 5.0

4. Numerical tests and computational details

The main deficiency of the Monte Carlo models based on the process of the direct imitation (Daniel 1978; Ménard 1989 etc.) is in the limited information extracting from the travel of a separate photon. The enormous number of photons and large computational time are usually needed to achieve reasonable accuracy.

In the approach described in the previous section, we try to avoid this defect including into consideration as much information on the geometry and physics of the problem discussed as we can. However, in case of our modified Monte Carlo scheme, there is a danger to get very small variance and incorrect results. Therefore, the thorough tests of the numerical code are necessary.

We tested our Monte Carlo code in the following ways.

(a). There should be no polarization from a homogeneous spherical shell. Our code gives the degree of linear polarization less than 10^{-8} % for $N_{\rm stat} \geq 1\,000$ photons. Theoretically, our algorithm should yield the zero polarization. Obtained non-zero values may be explained by the existence of the errors of the computer rounding of numbers during the calculations. It should be noted that to derive the value of $P \approx 0.01$ % for a spherical shell Daniel (1978) and Ménard (1989) needed $\approx 10^6$ and $5 \cdot 10^5$ photons, correspondingly.

(b). The polarization vanishes independently of the semiaxis ratio A/B if the shell is seen pole-on (i.e., $i = 0°$). In our model, this condition is automatically fulfilled because it is the basis of the method of symmetrized trajectories.

(c). For an optically thin spheroidal shell with Rayleigh particles, an approximate single scattering expression for the degree of polarization has been obtained (see e.g., Dolginov et al. 1979). We compared our results with this approximation for prolate and oblate shells with arbitrary values of A/B, i, and Λ and found satisfactory agreement. Note that as follows from Fig. 1, the single scattering approximation is valid if $\tau_{90}^{\rm ext} \lesssim 0.1$. The similar conclusion has been made by Daniel (1980a).

(d). For Mie scattering, the single scattering models of spheroidal shells have been considered by Zellner (1971; single size grains) and Voshchinnikov (1989; MRN mixture). Our results well agree with the results of these papers.

(e). We also constructed the separate numerical code based on the process of the direct imitation only and allowing to determine the Stokes vector after first and second scatterings in a spheroidal shell. A good agreement between two codes has been established.

In many cases, we detected a growth of the polarization degree after the second and several subsequent scatterings. This happens if the shell has a small or moderate optical thickness. Figure 2 shows how the polarization degree depends on the number of scatterings $N_{\rm scat}$ for the shells of various shape. The rise of the polarization after the second scattering is better seen for the strongly oblate shells. Such a behaviour has a simple explanation. The most distant layers of the oblate envelope give the largest contribution to the observed polarization, but some of the photons come there only after being scattered twice or more. This fact was briefly discussed by Celnikier & Lefèvre (1974) and Lefèvre & Daniel (1988).

When $\tau_{90}^{\rm ext}$ becomes large, the multiple scattering increases and the depolarization effects become dominating. The polarization degree rises to a maximum and then vanishes. For sufficiently large values of $\tau_{90}^{\rm ext}$, the polarization changes the sign because it is produced by the photons escaping out the polar parts of the shell. The photons scattered twice or more come from the shell edges, therefore the polarization decreases when we increase $N_{\rm scat}$ in optically thick envelopes (curve 6 in Fig. 2).

Table 1. The normalized intensity, the degree of linear polarization, and their relative statistical errors (Rayleigh scattering, $\Lambda = 0.5$, oblate shell, $A/B = 5$, $i = 90°$, $\tau_{90}^{\rm ext} = 1.0$)

$N_{\rm stat}$	I/I_*	$\sigma_{\rm I}$, %	P, %	$\sigma_{\rm P}$, %
10	0.4456	3.49	1.137	31.45
40	0.4474	1.52	1.733	19.40
160	0.4484	0.68	1.915	10.09
640	0.4555	0.41	2.287	4.57
2560	0.4578	0.22	2.331	2.42
10420	0.4580	0.11	2.332	1.22
40480	0.4576	0.06	2.322	0.62
161920	0.4577	0.03	2.314	0.31
647680	0.4575	0.01	2.319	0.15

The polarization reversal due to large optical thickness was found by Daniel (1980a) during Monte Carlo simulation of Thomson scattering. This feature was also noted by Hovenier (1971), Hansen & Travies (1974), Sobolev (1975), Loskutov (1990) for the case of multiple scattering in a plane slab. These authors used various (non Monte Carlo) numerical methods to solve the radiative transfer problem.

Figure 2 allows to estimate the optimum value of $N_{\rm scat}$ which we have to select to get the results with good accuracy. If we choose a too small number of scatterings, we may derive incorrect results. In the opposite case, we waste the computational time.

For our code, the computational time is proportional to the product of the scattering and photon numbers ($t \propto N_{\rm scat} \cdot N_{\rm stat}$). The true value of $N_{\rm stat}$ depends on the required accuracy of results. The variations of the relative statistical computational errors (σ) are proportional to $N_{stat}^{-1/2}$. Such a dependence is seen from Table 1 where the values of $\sigma_{\rm I}$ and $\sigma_{\rm P}$ have to become half as much in the subsequent rows from the top to the bottom.

In Table 2, we give the values of $N_{\rm stat}$ and $N_{\rm scat}$ necessary to reach the results with the relative error $\sigma_{\rm P} \leq 1.0\,\%$. It is obvious that the values of $N_{\rm scat}$ and $N_{\rm stat}$ are independent of the ratio A/B and the grain albedo, respectively. Note that the reduced values of $N_{\rm stat}$ for $A/B = 5$ are explained by the higher polarization degree in the comparison with shells having A/B = 1.1 or 10 (see Fig. 7).

For Mie scattering and standard MRN mixture (see Figs. 15 - 17), we used the values $N_{\rm stat}$ ranging from $\sim$ 3 000 photons in the red part of the spectrum to $\sim$ 300 000 photons in the ultraviolet in order to reach $\sigma_{\rm P} \leq 2.0\,\%$. For the mixtures containing only silicate (large albedo) or graphite (low albedo) grains (Fig. 18), the values of $N_{\rm stat}$ should be increased or decreased in 3 - 5 times, respectively.

5. Results and discussion

We have carried out the extensive calculations of the intensity and polarization for different parameters of CS shells.

Table 2. The numbers of photons and scatterings required to reach $\sigma_{\rm P}$ = 1.0 % (Rayleigh scattering, oblate shell, $i = 90°$)

Λ	$\tau_{90}^{\rm ext}$	A/B	$N_{\rm stat}$	$N_{\rm scat}$
0.1	0.1	1.1	12 000	1
		5.0	13 000	1
		10.0	18 000	1
	1.0	1.1	17 000	3
		5.0	15 000	3
		10.0	18 000	3
0.5	0.1	1.1	12 000	2
		5.0	13 000	2
		10.0	17 000	2
	1.0	1.1	18 000	4
		5.0	16 000	4
		10.0	19 000	4
1.0	0.1	1.1	11 000	2
		5.0	13 000	2
		10.0	17 000	2
	1.0	1.1	16 000	6
		5.0	16 000	6
		10.0	19 000	6

The observed ultraviolet or visual radiation of the star with shell (after correction for interstellar reddening) is the sum of the obscured stellar radiation and the scattered radiation

$$I(\lambda) = I_*(\lambda) \cdot {\rm e}^{-\tau_{\rm i}^{\rm ext}(\lambda)} + I_{\rm sca}(\lambda). \qquad (23)$$

Here, $\tau_{\rm i}^{\rm ext}(\lambda)$ is the optical path of the stellar radiation inside the shell in the direction of observer.

The first term of Eq. (23) describes the stellar brightness obscuring along the line of sight, and it may be found by the standard methods used for the calculations of the interstellar extinction curves. Then the wavelength dependence of $\tau_i^{\rm ext}(\lambda)$ is determined by the extinction of dust grains only.

The calculations of the scattered radiation are not so simple because they require the solution of the radiation transfer problem. The fraction of the scattered radiation depends on the shape and optical thickness of the shell, and the optical properties of dust grains (albedo and phase function). The behaviour of phase function is usually described by the asymmetry factor

$$g =< \cos\Theta >= \frac{1}{2}\int_{-1}^{1} R_{11}(\mu)\mu d\mu, \qquad (24)$$

which changes from -1 to +1.

We consider the intensity normalized by the stellar radiation intensity

$$I(\lambda)/I_*(\lambda) = {\rm e}^{-\tau_{\rm i}^{\rm ext}(\lambda)} + I_{\rm sca}(\lambda)/I_*(\lambda). \qquad (25)$$

For a star without shell, the ratio $I(\lambda)/I_*(\lambda)$ is equal to unity for all the wavelengths. The deviations of this ratio from unity indicate the absorption and scattering of the stellar radiation by CS dust grains.

The expression for the degree of linear polarization can be written as the ratio of the polarized radiation $I^{\rm p}_{\rm sca}(\lambda)$ to the total one

$$P(\lambda) = \frac{I^{\rm p}_{\rm sca}(\lambda)}{I_*(\lambda)\cdot {\rm e}^{-\tau_i^{\rm ext}(\lambda)} + I_{\rm sca}(\lambda)}. \tag{26}$$

In some cases (e.g., for Herbig Ae/Be stars with Algol-like minima), the stellar radiation may be absorbed additionally by CS dust clumps or clouds. The optical thickness of such clouds $\tau_{\rm 1}^{\rm ext}(\lambda)$ has to be added up to $\tau_i^{\rm ext}(\lambda)$ in Eqs. (23) and (26). If $\tau_{\rm 1}^{\rm ext}(\lambda) \gg 1$, we observe mainly the scattered radiation, i.e. CS shell is seen as a small reflection nebula. The scattered radiation restricts the amplitude of the stellar brightness variations due to CS extinction. This amplitude is equal to

$$\Delta m_{\rm max}(\lambda) = m_{\rm min}(\lambda) - m_{\rm max}(\lambda) =$$

$$= -2.5\cdot\log\frac{I_*(\lambda)\cdot {\rm e}^{-\tau_i^{\rm ext}(\lambda)-\tau_{\rm 1}^{\rm ext}(\lambda)} + I_{\rm sca}(\lambda)}{I_*(\lambda)\cdot {\rm e}^{-\tau_i^{\rm ext}(\lambda)} + I_{\rm sca}(\lambda)}$$

$$\approx -2.5\cdot\log\frac{I_{\rm sca}(\lambda)}{I_*(\lambda)\cdot {\rm e}^{-\tau_i^{\rm ext}(\lambda)} + I_{\rm sca}(\lambda)}. \tag{27}$$

The maximum degree of linear polarization can be written as follows

$$P_{\rm max}(\lambda) = I^{\rm p}_{\rm sca}(\lambda)/I_{\rm sca}(\lambda). \tag{28}$$

5.1. Rayleigh scattering

The models with Rayleigh scattering (with different albedo and the asymmetry factor g = 0) allow to study the cases of light scattering by electrons, molecules, and very small grains.

5.1.1. Intensity

The values of $I_{\rm sca}/I_*$ presented in Figs. 3 - 6 show that the scattered radiation can be a noticeable part of the direct stellar radiation. When the semiaxis ratio decreases, the ratio $I_{\rm sca}/I_*$ grows (Fig. 3). But this ratio changes weakly if we replace the prolate shell by the oblate one or vary the direction of observation (Figs. 3, 4). If i approaches 90°, the self-absorption effect appears (Fig. 4). In Figs. 3 and 4 we can see that the fraction of the scattered light increases with the optical thickness. However, this growth occurs only until $\tau_{90}^{\rm ext} \lesssim 1$, otherwise the ratio $I_{\rm sca}/I_*$ becomes smaller (Figs. 5, 6). This behaviour may be explained by the amplification of the multiple scattering effects and is known as the "accumulation effect" (Ivanov 1973). For optically thick shells, the ratio $I_{\rm sca}/I_*$ saturates, whereas the polarization changes the sign (see Fig. 2 and the discussion below).

It is evident that there is a strong correlation between the fraction of the scattered radiation and the grain albedo (see Fig. 6). ¿From the comparison of Fig. 3 with Fig. 6, we can conclude that the ratio $I_{\rm sca}/I_*$ should have a maximum for the case of the

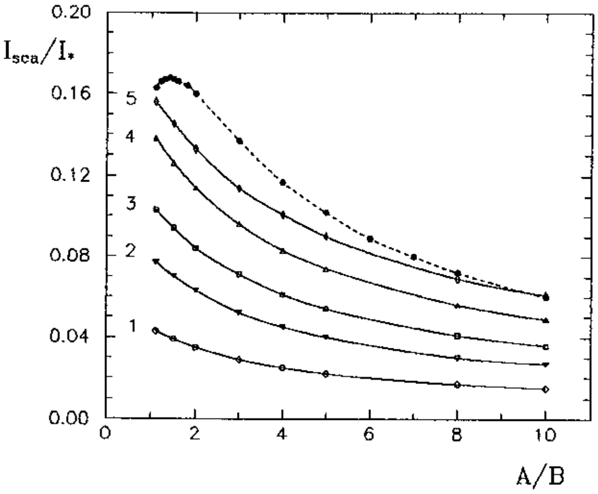

Fig. 3. Normalized scattered radiation as a function of the semiaxis ratio A/B (Rayleigh scattering, Λ = 0.5, i = 90°). Solid lines: oblate shell, 1 — $\tau_{90}^{\rm ext}$ = 0.1, 2 — $\tau_{90}^{\rm ext}$ = 0.2, 3 — $\tau_{90}^{\rm ext}$ = 0.3, 4 — $\tau_{90}^{\rm ext}$ = 0.5, 5 — $\tau_{90}^{\rm ext}$ = 1.0; dashed line: prolate shell, $\tau_{90}^{\rm ext}$ = 1.0

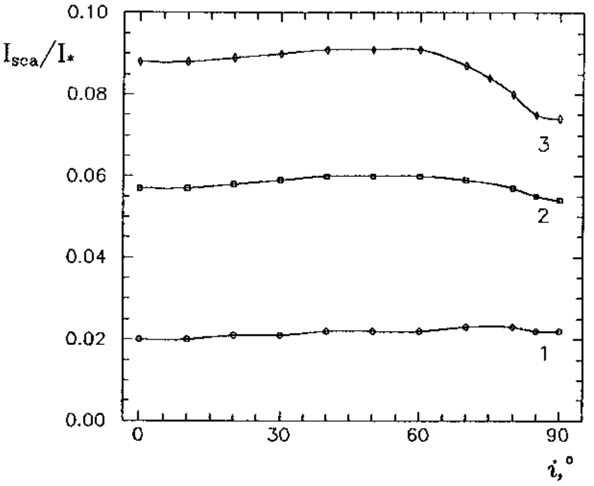

Fig. 4. Normalized scattered radiation as a function of the shell inclination angle (Rayleigh scattering, Λ = 0.5, oblate shell, A/B = 5). 1 — $\tau_{90}^{\rm ext}$ = 0.1, 2 — $\tau_{90}^{\rm ext}$ = 0.3, 3 — $\tau_{90}^{\rm ext}$ = 0.5

conservative scattering (Λ = 1) in the spherical shell with the optical thickness of about one. Our calculations gave the value $I_{\rm sca}/I_* \approx 37.1$ % for the spherical shell with $\tau_{90}^{\rm ext} \approx 1.1$. If $g \neq 0$ (the non-symmetric scattering), the maximum value can exceed 40 % (see Fig. 14). Then from Eq. (27) we can conclude that the variations of system's (star + shell) brightness can not exceed $\Delta m_{\rm max} \lesssim 0\overset{\rm m}{.}70$.

Some ways how to decrease the fraction of scattered radiation may be seen in Figs. 3 - 6. Other possibilities include the models with a central cavity free of dust and/or the inhomogeneous dust distribution with the density increasing outwards. Our preliminary results show that the presence of the dust-free cavity in the homogeneous shell leads to the values of $\Delta m_{\rm max}$ = $0\overset{\rm m}{.}7$, $1\overset{\rm m}{.}0$ and $1\overset{\rm m}{.}7$, if the ratio of the inner shell radius to the outer one is equal to 0.1, 0.5 and 0.9, respectively.

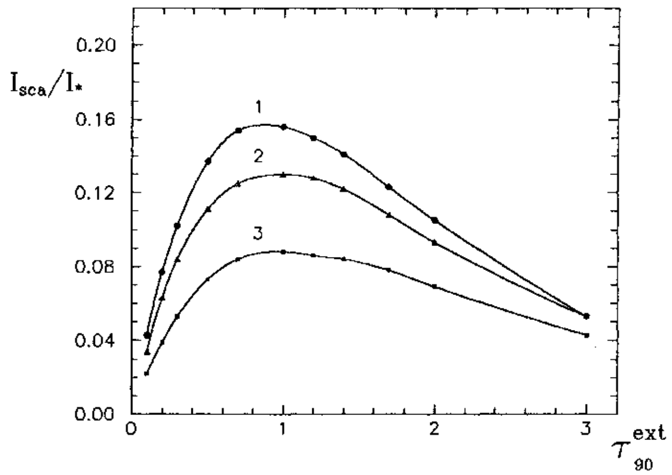

Fig. 5. Normalized scattered radiation as a function of the optical thickness of the shell (Rayleigh scattering, Λ = 0.5, oblate shell, i = 90°). 1 — A/B = 1.1, 2 — A/B = 2.0, 3 — A/B = 5.0

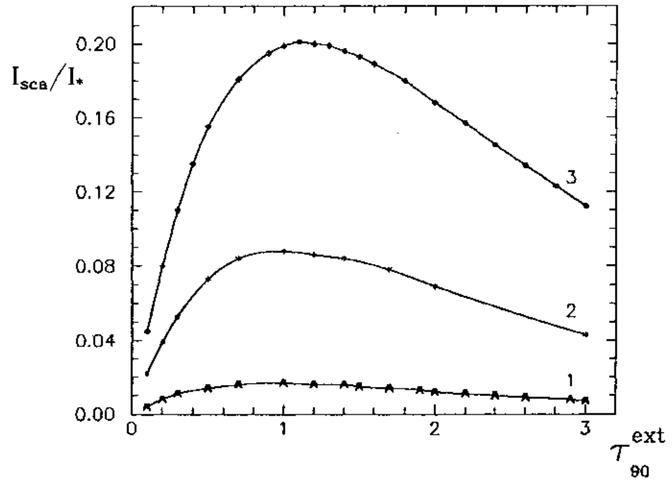

Fig. 6. Normalized scattered radiation as a function of the optical thickness of the shell (Rayleigh scattering, oblate shell, A/B = 5.0, i = 90°). 1 — Λ = 0.1, 2 — Λ = 0.5, 3 — Λ = 1.0

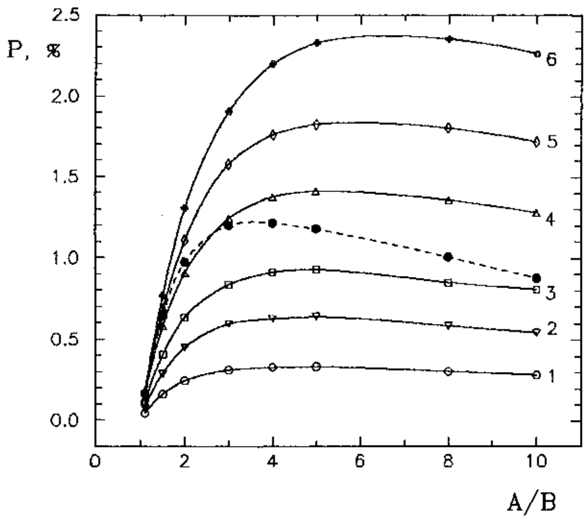

Fig. 7. Polarization degree as a function of the semiaxis ratio A/B (Rayleigh scattering, Λ = 0.5, i = 90°). Solid lines: oblate shell, 1 — τ_{90}^{ext} = 0.1, 2 — τ_{90}^{ext} = 0.2, 3 — τ_{90}^{ext} = 0.3, 4 — τ_{90}^{ext} = 0.5, 5 — τ_{90}^{ext} = 0.7, 6 — τ_{90}^{ext} = 1.0. Dashed line: prolate shell, τ_{90}^{ext} = 1.0

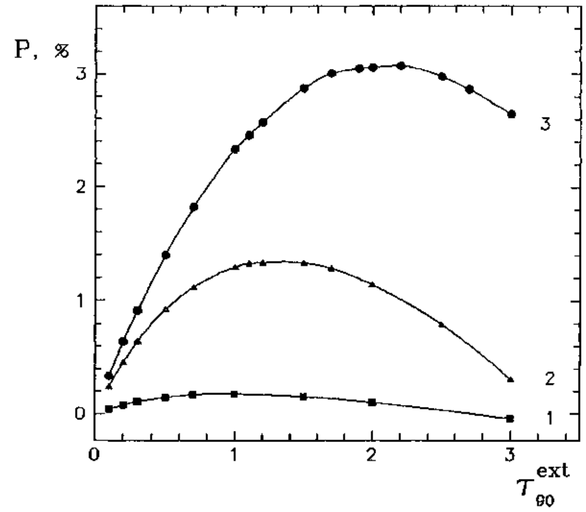

Fig. 8. Polarization degree as a function of the optical thickness of the shell (Rayleigh scattering, Λ = 0.5, oblate shell, i = 90°). 1 — A/B = 1.1, 2 — A/B = 2.0, 3 — A/B = 5.0

5.1.2. Polarization

The degree of linear polarization varies with the inclination angle i following approximately the well-known law $P \propto \sin^2 i$, obtained for optically thin shells (see e.g., Dolginov et al. 1979; Daniel 1980a and Fig. 1). The values of P are weakly dependent on the semiaxis ratio, if $A/B \geq 3$ and $\tau_{90}^{ext} \lesssim 0.3$ (Fig. 7).

The multiple scattering in optically thick shells leads to the decrease and reversal of polarization (curves 5, 6 in Fig. 2 and curve 1 in Fig. 8). Note also that the polarization is sensitive to the replacement of prolate shell by oblate one (cf. Figs. 3 and 7).

If we change τ_{90}^{ext} a correlation between the polarization degree and the fraction of the scattered radiation is clearly seen (cf. Figs. 5, 8 and Figs. 6, 9). But, naturally, the shell shape variations affect the scattered radiation and polarization in a different manner (Figs. 3 and 7).

Note also that the polarization degree can be greater than $\sim$ 6% (Fig. 9) if the stellar radiation is screened. It is known that in the case of conservative (Λ = 1) Rayleigh scattering in the optically thin plane slab, the polarization degree cannot exceed 33.3% (e.g., Dolginov et al. 1979). We tried to reach this limit considering the extremely oblate (pancake-like) shell seen edge-on. The following values of polarization degree have been obtained: P = 24.6% (for A/B = 100), P = 27.3% (A/B = 1 000), P = 28.9% (A/B = 10 000), and P = 30.3% (A/B = 100 000).

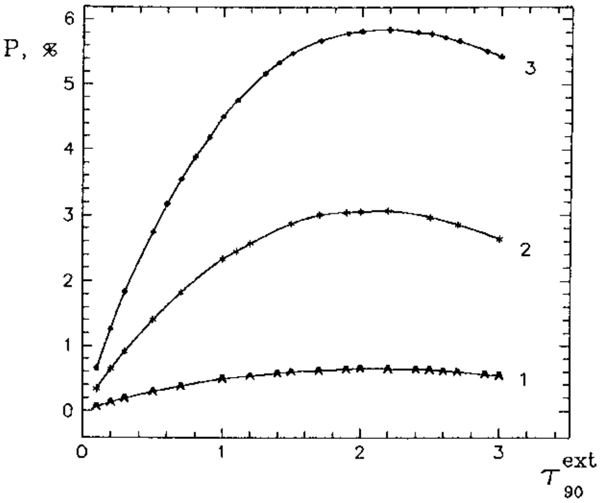

Fig. 9. Polarization degree as a function of the optical thickness of the shell (Rayleigh scattering, oblate shell, $A/B = 5.0$, $i = 90°$). 1 — $\Lambda = 0.1$, 2 — $\Lambda = 0.5$, 3 — $\Lambda = 1.0$

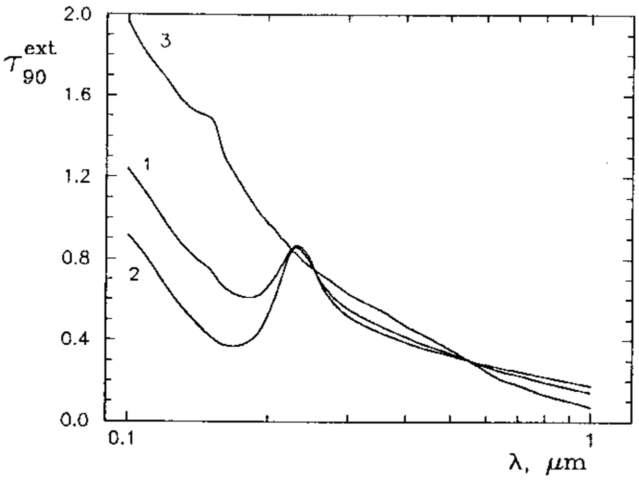

Fig. 10. Wavelength dependence of the optical thickness of the CS dust shell. 1 — standard MRN mixture ($n_{Si}/n_C = 1.07$), 2 — $n_{Si}/n_C = \infty$, 3 — $n_{Si}/n_C = 0$

5.2. *Mie scattering*

5.2.1. Optical properties of dust grains

In the case of Mie scattering, the calculations were made for silicate-graphite mixtures (see Sect. 2). Varying its parameters (a_-, a_+, q, n_{Si}/n_C), we can model dust shells around different stars. Three mixtures of dust grains were used: "standard" MRN mixture ($a_- = 0.005\,\mu$m, $a_+ = 0.25\,\mu$m, $q = 3.5$, $n_{Si}/n_C = 1.07$) and those mixtures consisting of either graphite ($n_{Si}/n_C = 0$) or silicate ($n_{Si}/n_C = \infty$) particles. The last two cases are important for the modelling of dust shells around carbon or oxygen stars. The standard MRN mixture may be used for young stars, where dust grains stay from the placental interstellar cloud.

We made calculations for the wavelength range from 1000 Å to 1 μm because some of hot young stars (e.g., Herbig Ae/Be stars) have been observed in the ultraviolet (Sitko 1981; Hartmann et al. 1993).

The optical constants for graphite and astronomical silicate were taken from the paper of Draine (1985). For all three mixtures, the asymmetry parameter g has the same behaviour decreasing from 0.6 - 0.7 in the ultraviolet to 0.2 - 0.3 in the red part of the spectrum. The grain albedo is equal to 0.4 in the range of λ = 0.1 - 0.2 μm. In the visual and near-ultraviolet parts of the spectrum, $\Lambda \approx 0.3$ - 0.4 (for graphite grains), ≈ 0.4 - 0.5 (for standard MRN mixture), and ≈ 0.8 - 0.9 (for silicate grains).

The wavelength dependence of the optical thickness $\tau_{90}^{ext}(\lambda)$ is shown in Fig. 10. It is normalized by the value of $\tau_{90}^{ext}(0.55\,\mu\text{m}) = 0.3$.

5.2.2. Intensity

In Fig. 11, we present the normalized intensity for the shells of different shape but with the same optical thickness. The fraction of the scattered radiation increases if the ratio A/B decreases (cf. Fig. 3). The obscured stellar radiation is the same in all

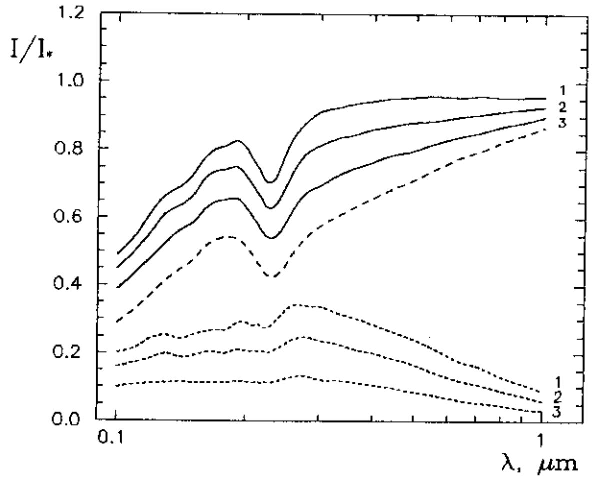

Fig. 11. Wavelength dependence of the normalized intensity (Mie scattering, standard MRN mixture, oblate shell, $\tau_{90}^{ext}(0.55\,\mu\text{m}) = 0.3$, $i = 90°$). 1 — $A/B = 1.1$, 2 — $A/B = 3.0$, 3 — $A/B = 10.0$. Solid lines: total radiation, short-dashed lines: scattered radiation, long-dashed line: obscured stellar radiation

the cases (long-dashed curve), but the total radiation may be wavelength independent in the visual part of the spectrum (solid curve 1).

It should also be noted that the variations of the shell shape affect the observed intensity of radiation and the polarization as well. Therefore, the spherical model for the shells around the Be star HD 45677 and Herbig Ae/Be star AB Aur posed by Sorrell (1989, 1990) seem to be doubtful because of the excess of the scattered radiation. The observed visual and ultraviolet polarization of the star HD 45677 (Coyne & Vrba 1976; Schulte-Ladbeck et al. 1992) indicates that Sorrel's model may be used only in the infrared wavelength region.

The optical thickness variations lead to the changes of the wavelength dependence of radiation. The sharp decrease of the

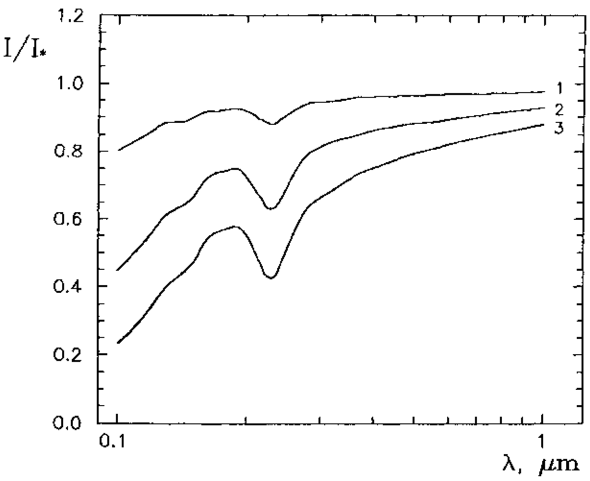

Fig. 12. Wavelength dependence of the normalized intensity (Mie scattering, $A/B=3, i=90°$). 1 — $\tau_{90}^{\rm ext}(0.55\,\mu{\rm m})=0.1$, 2 — $\tau_{90}^{\rm ext}(0.55\,\mu{\rm m})=0.3$, 3 — $\tau_{90}^{\rm ext}(0.55\,\mu{\rm m})=0.5$

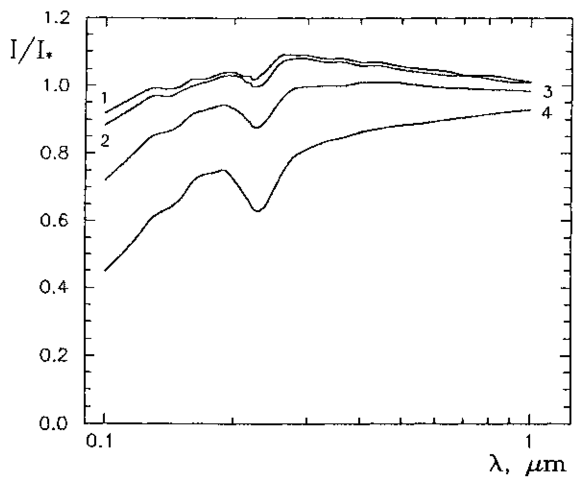

Fig. 13. Wavelength dependence of the normalized intensity (Mie scattering, $A/B=3$, $\tau_{90}^{\rm ext}(0.55\,\mu{\rm m})=0.3$). 1 — $i=0°$, 2 — $i=30°$, 3 — $i=60°$, 4 — $i=90°$

curve 3 in Fig. 12 at $\lambda < 0.2\,\mu$m is explained by the decrease of the fraction of the scattered radiation connected with the growth of the optical thickness. The effect of small particles (with size $a \lesssim 0.05\,\mu$m) is also important. If they are absent, the intensity has flat wavelength dependence (see Figs. 3, 4 in Voshchinnikov et al. 1993), which may be treated as the anomalous extinction curves (Steenman & Thé 1991).

Since the angle of observation i essentially affects only the obscured radiation but not the scattered one (see Eq. (23)), we derive the different wavelength dependence of intensity for CS shells observed pole-on and edge-on (Fig. 13). For the same optical thickness in the equatorial plane $\tau_{90}^{\rm ext}(\lambda)$, the effect of the shell orientation becomes noticeable only for $i \gtrsim 60°$. It is also seen that the total radiation of the star and shell can exceed the direct stellar radiation almost for all wavelengths (i.e., $I(\lambda) > I_*(\lambda)$, see curves 1, 2 in Fig. 13).

When the portion of the silicate particles in MRN mixture becomes large, the wavelength dependence of intensity differs from discussed above. Because of the large albedo of such grains, the fraction of scattered radiation grows significantly and can be larger than 40 % (Fig. 14). Then the ratio $I(\lambda)/I_*(\lambda)$ reaches the values up to ≈ 1.2 - 1.3 even for the shell seen edge-on. Such an excess of the total radiation in comparison with the direct stellar one leads to the appearance of the "negative" CS extinction, if the interstellar extinction is small or has been carefully excluded (see discussion in papers of Greenberg & Wang 1972 and Voshchinnikov et al. 1993). The accurate investigation of many T Tau and Herbig Ae/Be stars indicates the dominant role of the scattered light in their spectra (Hamann & Persson 1992). As a result, the interstellar extinction and stellar luminosity without the account of scattered radiation can be underestimated.

Note also that the results presented in Figs. 11 - 14 confirm the conclusion of Voshchinnikov et al. (1993) that the effect of dust shell on the observed radiation is the least in the wavelength region around 1 μm.

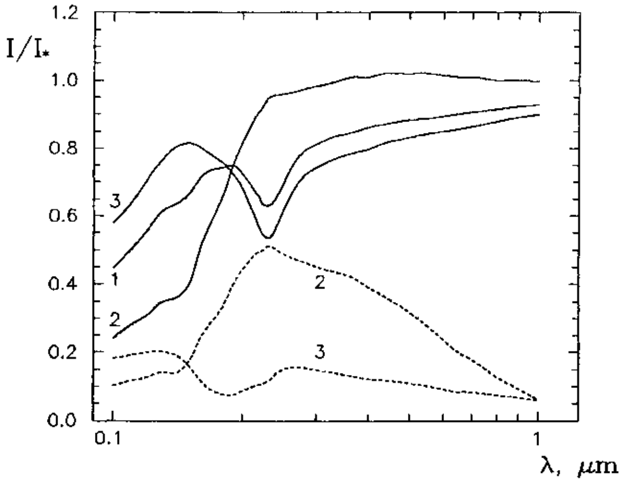

Fig. 14. Wavelength dependence of the normalized intensity (Mie scattering, $A/B=3$, $\tau_{90}^{\rm ext}(0.55\,\mu{\rm m})=0.3$, $i=90°$). 1 — standard MRN mixture, 2 — $n_{\rm Si}/n_{\rm C}=\infty$, 3 — $n_{\rm Si}/n_{\rm C}=0$. Solid lines: total radiation, dashed lines: scattered radiation

5.2.3. Linear polarization

The wavelength dependence of linear polarization are shown in Figs. 15 - 18. The evident growth of the polarization occurs increasing of the angle i (in all cases) and the optical thickness $\tau_{90}^{\rm ext}(\lambda)$ as well as the ratio A/B (to some extent). Because the polarization is nearly wavelength independent in the visual part of the spectrum, the curves of $P(\lambda)$ only does not allow to make a definite conclusion about the shell parameters.

The behaviour of polarization in the ultraviolet allows to estimate the chemical composition of dust grains and their minimum size. The presence of a large number of silicate grains (Fig. 18) or the absence of small grains (see Figs. 7, 8 in Voshchinnikov et al. 1993) leads to the decrease of polarization and even double reversal (i.e., the equatorial polarization transfers to the polar one and backwards). The similar result was obtained for

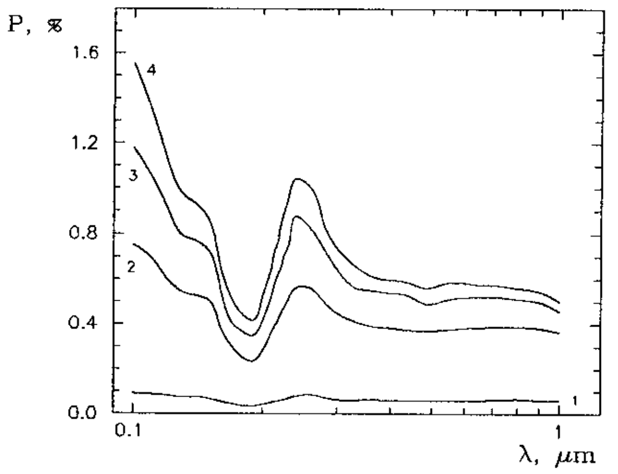

Fig. 15. Wavelength dependence of the linear polarization (Mie scattering, standard MRN mixture, oblate shell, $\tau_{90}^{\rm ext}(0.55\,\mu{\rm m}) = 0.3$, $i = 90°$). 1 — $A/B = 1.1$, 2 — $A/B = 2.0$, 3 — $A/B = 3.0$, 4 — $A/B = 5.0$

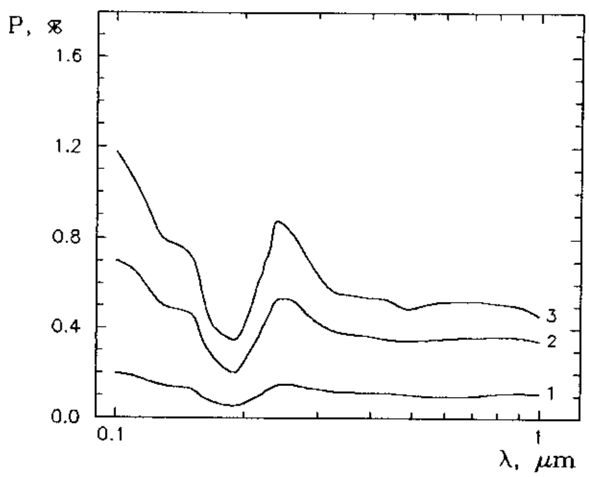

Fig. 17. Wavelength dependence of the linear polarization (Mie scattering, $A/B = 3$, $\tau_{90}^{\rm ext}(0.55\,\mu{\rm m}) = 0.3$). 1 — $i = 30°$, 2 — $i = 60°$, 3 — $i = 90°$

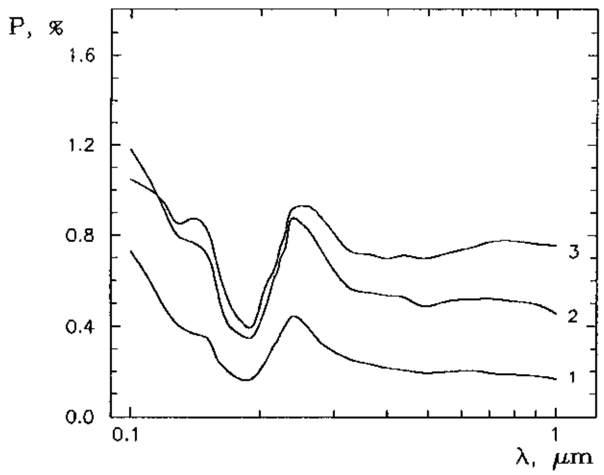

Fig. 16. Wavelength dependence of the linear polarization (Mie scattering, $A/B = 3, i = 90°$). 1 — $\tau_{90}^{\rm ext}(0.55\,\mu{\rm m}) = 0.1$, 2 — $\tau_{90}^{\rm ext}(0.55\,\mu{\rm m}) = 0.3$, 3 — $\tau_{90}^{\rm ext}(0.55\,\mu{\rm m}) = 0.5$

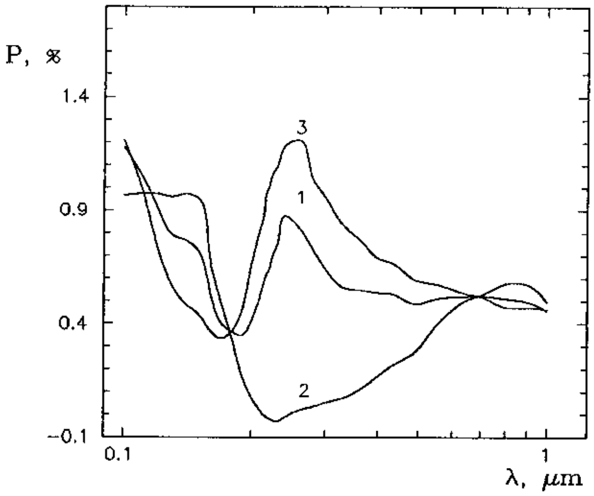

Fig. 18. Wavelength dependence of the linear polarization (Mie scattering, $A/B = 3$, $\tau_{90}^{\rm ext}(0.55\,\mu{\rm m}) = 0.3$, $i = 90°$). 1 — standard MRN mixture, 2 — $n_{\rm Si}/n_{\rm C} = \infty$, 3 — $n_{\rm Si}/n_{\rm C} = 0$

optically thick shells (see Figs. 2 and 8) but in those case the polarization sign changes only once.

The linear polarization sharply increases at $\lambda < 1800$ Å. If such a behaviour of polarization does not occur, we can conclude that the shell is seen almost pole-on (i.e., $i \lesssim 30°$, see curve 1 in Fig. 17) or the shell shape is close to the spherical one (curve 1 in Fig. 15). For both cases, the polarization is very small and cannot exceed 1 - 2 % even if the total star eclipse happens (Figs. 22, 23). In Figs. 15 - 18, another interesting peculiarity can be seen. It is connected with the fact that the polarization at $\lambda \approx 0.1\,\mu$m is larger than that near the ultraviolet bump around λ 2200 Å.

The behaviour of polarization discussed above allows to distinguish the intrinsic stellar polarization from the interstellar polarization. The interstellar polarization is known to follow the Serkowski law in the visual and has to drop in the ultraviolet. The first observations of the ultraviolet interstellar polarization (Wolff et al. 1993) show that for some stars there exists an excess of linear polarization in comparison with thatgiven by the Serkowski law. It may be explained by the presence of the CS dust shell producing the polarized radiation.

5.2.4. Circular polarization

The circular polarization of CS origin has been discovered for some T Tauri and FU Orionis stars (Nadeau & Bastien 1986; Bastien et al. 1989). The polarization degree reaches the values of $q_V \approx 0.06$ - 0.07 % in the red part of the spectrum. Bastien et al. (1989) connect its origin with the multiple scattering of light by spherical particles in the CS shells.

Indeed, in the case of Mie scattering, we derive the non-zero V component of the Stokes vector after the second scattering

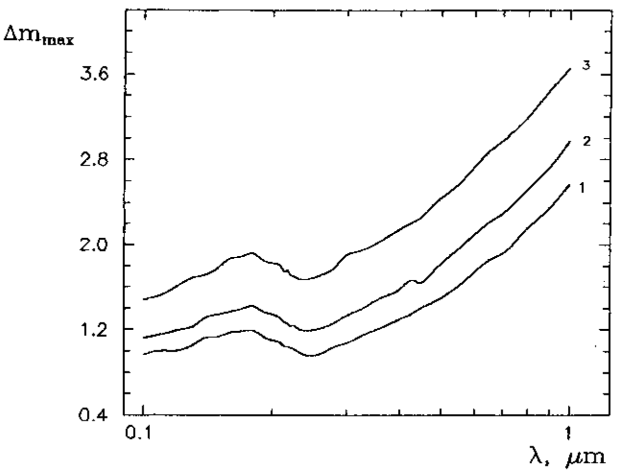

Fig. 19. Wavelength dependence of the maximum brightness variations (Mie scattering, standard MRN mixture, oblate shell, $\tau_{90}^{\rm ext}(0.55\,\mu{\rm m}) = 0.3, i = 90°$). 1 — $A/B = 1.1$, 2 — $A/B = 3.0$, 3 — $A/B = 10.0$

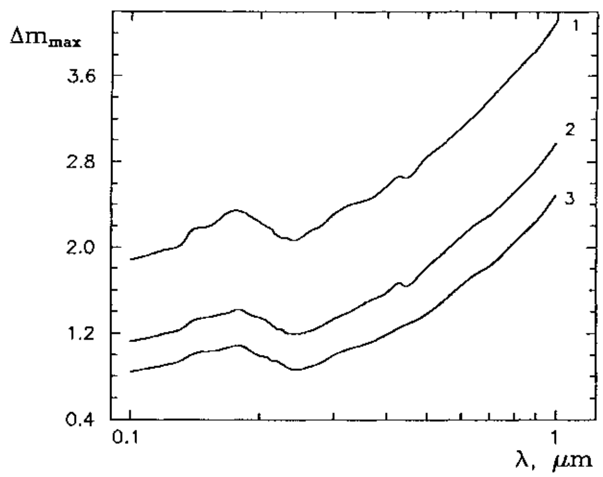

Fig. 20. Wavelength dependence of the maximum brightness variations (Mie scattering, $A/B = 3$, $i = 90°$). 1 — $\tau_{90}^{\rm ext}(0.55\,\mu{\rm m}) = 0.1$, 2 — $\tau_{90}^{\rm ext}(0.55\,\mu{\rm m}) = 0.3$, 3 — $\tau_{90}^{\rm ext}(0.55\,\mu{\rm m}) = 0.5$

(see Eq. (7)). However, our calculations show that this component is negligible. The derived values of the circular polarization are $q_{\rm V} \approx 0.001$ - 0.005 % with the relative errors ~ 100 % (such values are obtained if the error of linear polarization is $\sigma_{\rm P} \leq 2.0\,\%$, see Sect. 4). The maximum value $q_{\rm V} \approx 0.01$ % was derived at ultraviolet wavelengths for nearly spherical shell ($A/B = 1.1$). These results show that the multiple light scattering by spherical particles in an homogeneous spheroidal shell cannot create an essential circular polarization. The polarization may be comparable with the observed ones (or even larger) if the direct stellar radiation and/or a part of the shell is screened from an observer. The high circular polarization may also arise due to light scattering by non-spherical particles. The modelling of polarization maps (Ménard 1989; Fischer 1993) shows that the circular polarization can be significant for the outer parts of the reflection nebulae or large CS shells which may be resolved in a telescope.

5.3. Circumstellar shells with clumps

5.3.1. Maximum brightness variations

Using Eq. (27), we can also estimate the limits of star brightness variations. As it is seen from Figs. 19 - 21, they are $\lesssim 1^{\rm m}$ - $2^{\rm m}$ in the far ultraviolet. That means that a CS cloud with the visual extinction $A_{\rm V} \approx 0^{\rm m}\!.5$ - $1^{\rm m}\!.0$ and the standard extinction law can screen the direct stellar radiation from the observer. In the red part of the spectrum, the total star eclipse occurs when the cloud extinction $A_{\rm V} \gtrsim 4^{\rm m}$ - $8^{\rm m}$. Figures 19 - 21 show that maximum brightness variation is in inverse ratio to the fraction of scattered radiation, i.e. $\Delta m(\lambda)$ increases with the decrease of the optical thickness, grain albedo, and the ratio B/A.

The results presented in Figs. 19 - 21 can be used directly for the explanation of the photometric behaviour of Herbig Ae/Be stars with Algol-like variations of brightness (UX Ori, WW Vul, CQ Tau, etc.). Their brightness variations can reach up to $2^{\rm m}\!.5$ in the V band (see discussion in Voshchinnikov 1989). The comparison of these values with Figs. 19 - 21 shows that we could hardly produce so large variations using dust mixtures primarily consisting of silicate grains or quasi-spherical shell with a moderate optical thickness. Note also that the large intrinsic polarization of Herbig Ae/Be stars observed by Grinin et al. (1991) disagrees with spherical shell models.

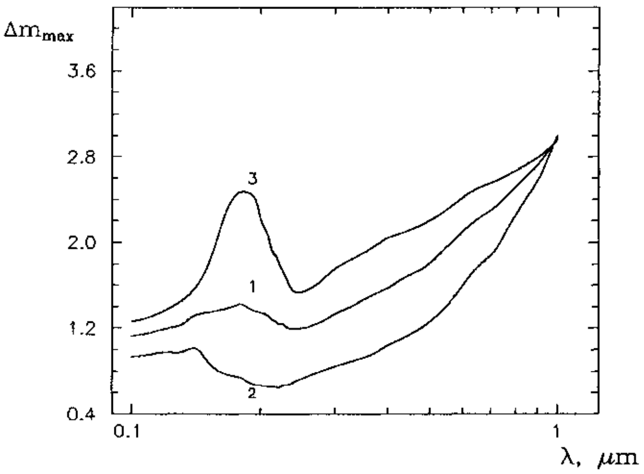

Fig. 21. Wavelength dependence of the maximum brightness variations (Mie scattering, $A/B = 3$, $\tau_{90}^{\rm ext}(0.55\,\mu{\rm m}) = 0.3$, $i = 90°$). 1 — standard MRN mixture, 2 — $n_{\rm Si}/n_{\rm C} = \infty$, 3 — $n_{\rm Si}/n_{\rm C} = 0$

5.3.2. Maximum linear polarization

During the eclipse of star by a dense dust cloud or clump, the polarization increases. It reaches the maximum when the optical thickness of the clump is very large (i.e., the first term in the denominator in Eq. (26) vanishes). The wavelength dependence of the maximum polarization $P_{\rm max}(\lambda)$ is shown in Figs. 22 - 24 for several values of A/B, i, and $n_{\rm Si}/n_{\rm C}$. The polarization grows from visual to red wavelengths (as in reflection nebulae) and can reach 8 - 10 %. It has a minimum at wavelengths $\lambda\lambda = 0.18$ -

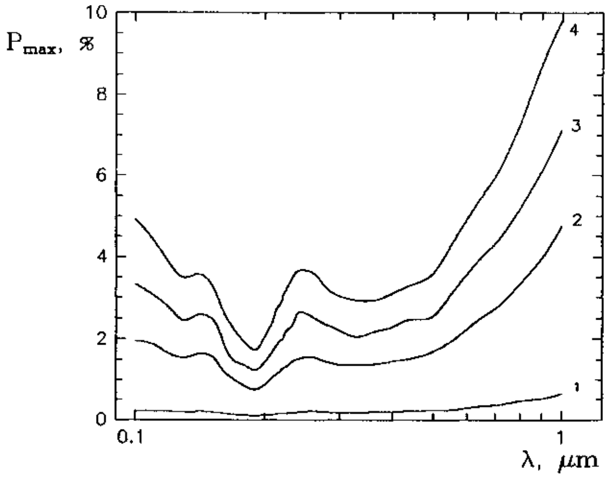

Fig. 22. Wavelength dependence of the maximum polarization (Mie scattering, standard MRN mixture, oblate shell, $\tau_{90}^{ext}(0.55\,\mu m) = 0.3$, $i = 90°$). 1 — $A/B = 1.1$, 2 — $A/B = 2.0$, 3 — $A/B = 3.0$. 4 — $A/B = 5.0$

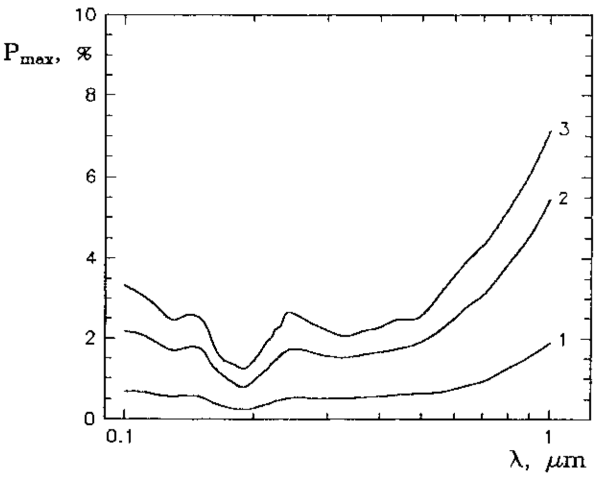

Fig. 23. Wavelength dependence of the maximum polarization (Mie scattering, $A/B = 3$, $\tau_{90}^{ext}(0.55\,\mu m) = 0.3$). 1 — $i = 30°$, 2 — $i = 60°$, 3 — $i = 90°$

0.20 μm and grows in the far ultraviolet (except for the shell with graphite particles, Fig. 24).

The analysis of the observations of Herbig Ae/Be stars shows (see e.g., Voshchinnikov & Grinin 1992; Friedemann et al. 1993) that the CS clouds consist of submicron particles which produce the selective extinction. Therefore, it is hard to expect that the stellar radiation may be suppressed from the far ultraviolet to the infrared wavelengths simultaneously. However, the total eclipse may easily happen in the blue or ultraviolet part of the spectrum.

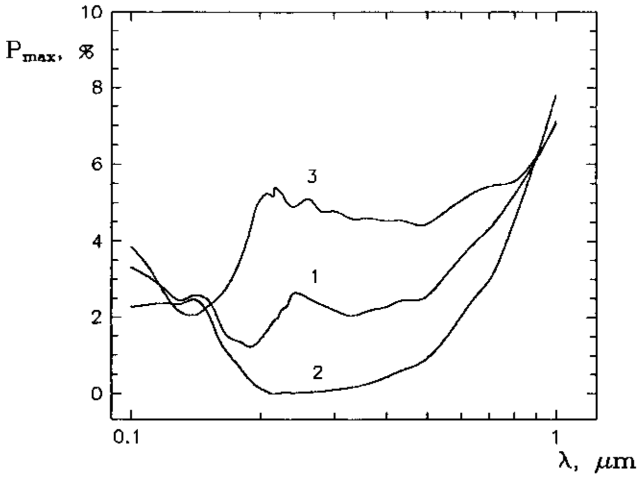

Fig. 24. Wavelength dependence of the maximum polarization (Mie scattering, $A/B = 3$, $\tau_{90}^{ext}(0.55\,\mu m) = 0.3$, $i = 90°$). 1 — standard MRN mixture, 2 — $n_{Si}/n_C = \infty$, 3 — $n_{Si}/n_C = 0$

Note that the variations of the optical thickness influence only slightly on the values of $P_{max}(\lambda)$ because both $I_{sca}^{p}(\lambda)$ and $I_{sca}(\lambda)$ grow with the increase of $\tau_{90}^{ext}(\lambda)$, keeping its ratio nearly constant (see Eq. (28)).

In order to describe the behaviour of polarization on the intermediate levels of star brightness (between the values given by Eqs. (26) and (28)), the approximate expression presented in the paper of Grinin et al. (1988) may be used.

6. Conclusions

We can summarize the results of our paper as follows.

1. On the basis of recently developed modification of the Monte Carlo approach (the method of symmetrized trajectories), we created a numerical code for the transfer of polarized radiation in circumstellar shells. It allows to study light scattering by dust grains in prolate or oblate spheroidal shells of moderate optical thickness ($\tau \lesssim 5$ - 8) seen at various angles. The calculations do not require the extremely large computational efforts. It needs 15 000 - 18 000 photons only to get the linear polarization degree with the relative error less than 1 % for the shell with the optical thickness $\tau = 1.0$ seen edge-on.

The extensive calculations were performed for the cases of Rayleigh scattering (grain albedo $\Lambda = 0.1, 0.5$, and 1.0) and Mie scattering (silicate-graphite mixtures, the wavelength range $\lambda\lambda$ = 1000 Å - 1 μm).

2. The contribution of the scattered radiation to the observed one is most essential in the visual and ultraviolet parts of the spectrum. It grows with increasing Λ and decreasing the semi-axis ratio A/B of the shell. The effect of the multiple scattering appears if the optical thickness of the shell $\tau > 1$. It leads to a decrease of the fraction of scattered radiation and to a change of the polarization sign if $\tau \gtrsim 3$.

3. The ratio of the scattered radiation intensity to the stellar one, I_{sca}/I_*, can reach ≈ 0.3 - 0.4 and has a maximum at $\lambda \approx 2000$ - 3000 Å. In some cases, the scattered radiation and

circumstellar extinction may lead to wavelength independent extinction curves which cannot be analyzed by colour excess method. If the fraction of the scattered radiation is large and the ratio $(I_{sca} + I_*)/I_* > 1$, the "negative" extinction occurs.

4. The degree of the linear polarization usually does not exceed 1 - 2 % and has a weak wavelength dependence in the visual and red parts of the spectrum. At the ultraviolet wavelengths, the polarization has a maximum in the region of the bump ($\lambda \approx 2200$ Å) and a minimum at $\lambda \approx 1800$ - 2000 Å. If the observations do not show such a growth of polarization at $\lambda < 1800$ Å, we can conclude that the visible shape of the shell is close to circular. It means that the spheroidal shell is seen nearly pole-on ($i < 30°$) or it has a quasi-spherical shape.

The flat polarization spectra in the ultraviolet may be also explained by a low fraction of very small particles in a grain mixture. In some cases, it leads to double polarization reversal.

5. If the stellar radiation is screened by dense circumstellar clump, we observe the fading of the stellar brightness with the simultaneous increase of the polarization degree. If the clump is very dense, practically only the radiation scattered by circumstellar grains will be observed. The upper limit of the stellar brightness variations will be 1^m - 2^m in the ultraviolet and 3^m - 4^m in the red part of the spectrum. The maximum degree of linear polarization grows with wavelength and reaches 8 - 10 %.

Acknowledgements. We wish to thank V.B. Il'in for many helpful comments. We are grateful to A. Schneider, A.B. Men'shchikov, and the anonymous referee for the careful reading of the manuscript. This research was supported in part by a grant of the Academy of Sciences of the former Soviet Union and by the Russian Scientific Committee grant G 01.3.5.10. The calculations have been carried out mainly on the PC/AT 486 computer out of the Fund for East Europe Sponsorship 12161.

References

Angel J.R.P., 1969, ApJ 158, 219
Bastien P., 1988, Polarization Properties of T Tauri Stars and Other Pre-Main Sequence Objects. In: G.V.Coyne et al. (eds.), Polarized Radiation of Circumstellar Origin. Tucson, Univ. Arizona Press, p.541
Bastien P., Ménard F., 1988, ApJ 326, 334
Bastien P., Robert C., Nadeau R., 1989, ApJ 339, 1089
Berrilli F., Corciulo G., Ingrosso G., Lorenzetti D., Nisini B., Strafella F., 1992, ApJ 398, 254
Celnikier L.M., Lefèvre J., 1974, A&A 36, 429
Chandrasekhar S., 1950, Radiative Transfer. Oxford Univ. Press, Oxford
Coyne G.V., Vrba F.J., 1976, ApJ 207, 790
Daniel J.-Y., 1978, A&A 67, 345
Daniel J.-Y., 1980a, A&A 86, 198
Daniel J.-Y., 1980b, A&A 87, 204
Daniel J.-Y., 1982, A&A 111, 58
Dolginov A.Z., Gnedin Yu.N., Silant'ev N.A., 1979, Propagation and Polarization of Radiation in Cosmic Medium. Nauka, Moscow, p.194
Draine B.T., 1985, ApJS 57, 587
Fischer O., 1993, Ph.D. Thesis, Jena University
Fischer O., Henning Th., Yorke H.W., 1993, A&A, in press
Friedemann C., Reimann H.-G., Gürtler J., Tóth V., 1993, A&A, 277, 184
Greenberg J.M., Wang R.T., 1972, Mem. Soc. Roy. Liège 6 ser. 3, 197
Grinin V.P., Kiselev N.N., Minikulov N.Kh., Chernova G.P., 1988, Pis'ma AZh, 14, 514
Grinin V.P., Kiselev N.N., Minikulov N.Kh., Chernova G.P., Voshchinnikov N.V., 1991, Ap&SS 186, 283
Gürtler J., Henning Th., Krügel E., Chini R., 1991, A&A 252, 801
Hamann F., Persson S.E., 1992, ApJ 394, 628
Hansen J.E., Travis, L.D., 1974, Space Sci. Rev. 16, 527
Hartmann L., Kenyon S.J., Calvet N., 1993, ApJ 407, 219
Höflich P., 1991, A&A 246, 481
Hovenier J.W., 1971, A&A 13, 7
Hovenier J.W., van der Mee C.V.M., 1983, A&A 128, 1
Ivanov V.V., 1973, Transfer of Radiation in Spectral Lines. NBS Publ. 385, US Govt. Printing Office, Washington
Jones T.W., Merrill K.M., 1976, ApJ 209, 509
Karjukin V.V., 1984, Vestnik Leningrad Univ. N1, 93
Karjukin V.V., 1992, In: Model Oriented Data-Analysis. A Survey of Recent Methods, Proc. 3th IIASA-workshop in St. Petersburg, 25-30 May, in press
Lefèvre J., Daniel J.-Y., 1988, Numerical Simulation of the Polarization in Late-Type Variable Star Envelopes. In: G.V.Coyne et al. (eds.), Polarized Radiation of Circumstellar Origin. Tucson, Univ. Arizona Press, p.523
Loskutov V.M., 1990, Vestnik Leningrad Univ. N1, 91
Marchuk G.I., Mikhailov G.A., Nazaraliev M.A., Darbinjan D.A., Kargin B.A., Elepov B.S., 1980, The Monte Carlo Methods in Atmospheric Optics. Springer-Verlag, New York
Mathis J.S., Rumpl W., Nordsieck K.H., 1977, ApJ 217, 425
Ménard F., 1989, Ph.D. Thesis, Université de Montréal
Nadeau R., Bastien P., 1986, ApJ 307, L5
Natta A., Palla F., Butner H.M., Evans N.J.II, Harvey P.M., 1993, ApJ 406, 674
Rodriguez L.F., Cantó J., Torrelles J.M., Gómez J.F., Ho P.T.P., 1992, ApJ 393, L29
Rowan-Robinson M., 1982, MNRAS 201, 289
Rydgren A.E., Cohen M., 1985, Young Stellar Objects and their Circumstellar Dust: an overview. In: D.C.Black, M.S.Mattews (eds.), Protostars and Planets II. Tucson, Univ. Arizona Press, p.371
Schulte-Ladbeck R., Shepherd D.S., Nordsieck K.H., Code A.D., Anderson C.M., Babler B.L., Bjorkman K.S., Clayton G.C., Magalhães A.M., Meade M.R., Whitney B.A., 1992, ApJ 401, L105
Shawl S.J., 1974, Polarimetry of Late-Type Stars. In: T.Gehrels (ed.), Planets, Stars and Nebulae studied with photopolarimetry. Tucson, Univ. Arizona Press, p.821
Sitko M.L., 1981, ApJ 247, 1024
Sloan G.C., Grasdalen G.L., Levan P.D., 1993, ApJ 404, 328
Sobolev V.V., 1975, Light Scattering in Planetary Atmospheres. Pergamon Press, Oxford
Sobol' I.M., 1973, Numerical Monte Carlo Methods. Nauka, Moscow
Sorrell W.H., 1989, MNRAS 241, 89
Sorrell W.H., 1990, ApJ 361, 150
Steenman H., Thé P.S., 1991, Ap&SS 184, 9
Tamura M., Hasegawa T., Ukita N., Gatley I., McLean I.S., Burton M.G., Rayner J.T., McCaughrean M.J., 1988, ApJ 326, L17
Voshchinnikov N.V., 1989, Afz 30, 313
Voshchinnikov N.V., Grinin V.P., 1992, Afz 34, 84
Voshchinnikov N.V., Grinin V.P., Karjukin V.V., 1993, A&A, in press
Weintraub D.A., Kastner J.H., Zuckermann B., Gatley I., 1992, ApJ 391, 784
Whitney B.A., Hartmann L., 1992, ApJ 395, 529
Wolff M.J., Clayton G.C., Meade M.R., 1993, ApJ 403, 722
Zellner B., 1971, AJ 76, 651

This article was processed by the author using Springer-Verlag LaTeX A&A style file version 3.